Supporting information for

Solvent-responsive solid/liquid phase transitions of condensates depend on trade-off molecular interactions

Feipeng Chen[1,4,7], Yongxu Han[2], Huiyanchen Li[4], Xiufeng Li[4,5], Wei Guo[1,4], Changjin Wu[1,4], Jiang Xia[2], Xiangze Zeng[3*], Ho Cheung Shum[1,4,6*]

[1]Department of Mechanical Engineering, The University of Hong Kong, Pokfulam Road, Hong Kong (SAR) 999077, China

[2]Department of Chemistry, The Chinese University of Hong Kong, Shatin, Hong Kong, China

[3]Department of Physics, Hong Kong Baptist University, Kowloon Tong, Hong Kong, China

[4]Advanced Biomedical Instrumentation Centre, Hong Kong Science Park, Shatin, New Territories, Hong Kong (SAR) 999077, China

[5]College of Food Science and Technology, Nanjing Agricultural University, Nanjing, 210095, Jiangsu, China

[6]Department of Biomedical Engineering & Department of Chemistry, City University of Hong Kong, Kowloon, Hong Kong, China.

[7]Current address: Department of Chemical and Biological Engineering, Northwestern University, Evanston, Illinois 60208, United States

*Corresponding author. Email: xiangzezeng@hkbu.edu.hk; ashum@cityu.edu.hk

Supplementary Table 1: Inconsistent effects of organic solvents on the phase transitions of coacervates or condensates reported in literature.

Material	Organic Solvent	Effect	reference
amyloid-β (Aβ)	Ethanol	SLPT	[1, 2]
Lysozyme	Ethanol	SLPT	[3, 4]
PSS/PVBTMA	Ethanol, ethylene glycol	SLPT	[5]
PAAcat/ QCS-Tf2N	DMSO	SLPT	[6]
PSS/P3BImHTBr	Tetrahydrofuran	SLPT	[7]
keratin-8 protein	Ethanol	LSPT	[8]
$_{179}$CVNITV$_{184}$ protein	Ethanol	LSPT	[9]
Chitosan/ Hyaluronic Acid	Ethanol, methanol	LSPT	[10]
PDDPC/PVS; PDDPC/PAA	Ethanol	LSPT	[11]
BPEI/PAA	Ethanol, methanol, etc.	LSPT	[12]

PSS: Poly(sodium 4-styrenesulfonate)

PVBTMA: Poly[(vinylbenzyl)trimethylammonium chloride]

PAAcat: Poly(acrylic acid) functionalized with catechols

QCS-Tf2N: Chitosan ion-paired with bis(trifluoromethane-sulphonyl)imide

P3BImHTBr: poly[3-[6′-(N-butylimidazolium)-hexyl]thiophene]bromide

PDDPC: Poly(N,N-dimethyl-3,5-dimethylene piperidinium chloride)

PVA: Polyvinylamine

PAA: Poly(acrylic acid)

PVS: poly(vinylsulfonic acid, sodium salt)

BPEI: branched poly(ethylene imine)

Supplementary Table 2: Plasmids, vectors, and amino acid sequence of RGG and ELP proteins

Protein	Plasmids	Vector	Sequence
RGG	RGGRGG-EGFP	Pet 21 a	MKGSSHHHHH HVDAHIVMVD AYKPTKLDGH GVGVPGVGVP GVGVPGEGVP GVGVPGVGVP GVGVPGVGVP GEGVPGVGVP GVGVPGVGVP GVGVPGEGVP GVGVPGVGEL PEDLGTGLLE ALLRGDLAGA EALFRRGLRF WGPEGVLEHL LLPVLREVGE AWHRGEIGVA EEHLASTFLR ARLQELLDLA GFPPGPPVLV TTPPGERHEI GAMLAAYHLR RKGVPALYLG PDTPLPDLRA LARRLGAGAV VLSAVLSEPL RALPDGALKD LAPRVFLGGQ GAGPEEARRL GAEYMEDLKG LAEALWLPRG PEKEAITSVP GVGVPGVGVP GEGVPGVGVP GVGVPGVGVP GVGVPGEGVP GVGVPGVGVP GVGVPGVGVP GEGVPGVGVP GVGVPGGLLD AHIVMVDAYK PTKLEWKK
ELP	SpyTag-Elp-CarH-Elp-SpyTag	pQE-80L	MESNQSNNGG SGNAALNRGG RYVPPHLRGG DGGAAAAASA GGDDRRGGAG GGGYRRGGGN SGGGGGGGYD RGYNDNRDDR DNRGGSGGYG RDRNYEDRGY NGGGGGGGNR GYNNNRGGGG GGYNRQDRGD GGSSNFSRGG YNNRDEGSDN RGSGRSYNND RRDNGGDGES NQSNNGGSGN AALNRGGRYV PPHLRGGDGG AAAAASAGGD DRRGGAGGGG YRRGGGNSGG GGGGGYDRGY NDNRDDRDNR GGSGGYGRDR NYEDRGYNGG GGGGGNRGYN NNRGGGGGGY NRQDRGDGGS SNFSRGGYNN RDEGSDNRGS GRSYNNDRRD NGGDG

Supplementary Note 1: Estimation of different driving forces affected by the introduction of organic solvents.

Molecular interactions, such as electrostatic interaction, cation - π, and π - π, are the main driving forces for the complex coacervation. Therefore, to investigate the effects of solvents on complex coacervations, we further examine the changes of molecular interaction energy based on theoretical models upon the introduction of organic solvents. For coacervates formed by oppositely charged polyelectrolytes with relatively hydrophilic sidechains, the main driving force for the phase separation is assumed to be the electrostatic interaction. For disconnected ions with diameters $\sigma = \nu^{1/3}$, electrostatic free energy is given by a generalized Debye−Hückel expression as[13, 14],

$$f_{el} = -\frac{1}{4\pi\nu}\left[\ln(1+\kappa\sigma) - \kappa\sigma + \frac{(\kappa\sigma)^2}{2}\right] \quad (1)$$

where κ is the inverse Debye screening length[15] given by $\kappa\sigma = \sqrt{4\pi(l_B/\sigma)\sum\phi_i f_i}$ with Bjerrum length $l_B = e^2/4\pi k_B T\varepsilon_0\varepsilon_s$ (where f_i is the charge density of polymers or salts, e is the elementary charge, ε_0 is the vacuum permittivity, ε_s is the dielectric constant of the solvent). In the dilute limit, $\phi_i \to 0$, Eq. 1 reduces to well-known Debye−Hückel correlation free energy as used in Voorn-Overbeek (VO) theory[16],

$$f_{el} = -\kappa^3/12\pi. \quad (2)$$

For simplicity, Eq. 2 is used to calculate electrostatic free energy in our work. Based on Eq. 2, f_{el} scales with $(l_B)^{3/2}$ and thus $(\varepsilon_r)^{-3/2}$, as $f_{el} \propto (l_B)^{3/2} \propto (\varepsilon_r)^{-3/2}$. This indicates the electrostatic interaction is enhanced when the the dielectric constant of solvent decease upon the introduction of organic solvents into water.

For coacervates formed by oppositely charged polyelectrolytes with aromatic residues, cation-π and π - π interactions play important roles in the complex coacervation[17, 18]. Apart from electrostatic interactions between two charges, all other interactions involve polarization effects for molecules of polarizability α. This is because all atoms and molecules are polarizable and the polarizability arise from the displacement of its negatively charged electron cloud relative to the positively charged nucleus under the influence of an external electric field [19]. Therefore, the energetic

contributions from these short-range interactions in a solvent medium can be modeled as [19],

$$f_{sr} = -\frac{3kT}{r^6}\left(\frac{\varepsilon_p - \varepsilon_s}{\varepsilon_p + 2\varepsilon_s}\right)^2 \alpha^6, \quad (4)$$

where ε_p and ε_s are the dielectric consant of moleucles and solvents, respectively. Based on the Eq. 4, it is shown that f_{sr} scales with $\left(\frac{\varepsilon_p - \varepsilon_s}{\varepsilon_p + 2\varepsilon_s}\right)^2$. The dielectric constant of water ε_w and ethanol ε_e at room temperature ($T = 20$ ℃) are 80.2 and 24.3, respectively. The dielectric constant of a mixture of water and ethanol can be calculated as $\varepsilon_s = \varphi_e \varepsilon_e + (1 - \varphi_e)\varepsilon_w$ [20]. With this, ε_s decrease monotonically with increasing φ_e upon the introduction of ethanol into water. Therefore, it is found that f_{sr} continues to decrease with decreasing value of ε_s, suggesting that the strength of cation-π and π - π interactions are reduced in the presence of organic solvents.

Supplementary Note 2: Time-ethanol and time-temperature superposition reveals changes in interaction strength

To better understand the variations in physical properties and molecular interactions within coacervates affected by alcohols, we employ a superposition method to analyze the rheology data. Superposition is a well-known rheological principle to study the response of viscoelastic materials over a broad range of frequencies [10, 21]. We first conduct frequency sweeps on two exemplary complex coacervates, PAA/PDMAEMA and PVS/PVBTMA, at different volume fractions of ethanol and temperatures. The overall shape of rheology curves of these coacervates is typical of polymer melt with viscoelastic properties being dominated by the loss modulus (G'') at low frequency and the storage modulus (G') at high frequency (Supplementary Fig. 7 and Supplementary Fig. 8).

Consistent with the previous observations and our hypothesis, the presence of ethanol leads to significant decrease in $G'$and G'' of PVS/PVBTMA coacervates containing aromatic residues, whereas it increases $G'$and G'' of PAA/PDMAEMA coacervates lacking aromatic residues (Supplementary Fig. 7). By employing a time-ethanol superposition where the frequency and modulus are multiplied by a critical relaxation time (τ_c) and a vertical shift factor b_φ, frequency sweeps conducted at different volume fractions of ethanol (φ_e) are rescaled onto master curves (Supplementary Fig. 9a and Supplementary Fig. 9b). The successful application of time-alcohol superpositions implies that these coacervates remain self-similar and homogeneous structures. Therefore, studying the viscoelastic properties of coacervates at different conditions is equivalent to examining them at different time scales [10, 22]. Intriguingly, in the time-ethanol superpositions, τ_c and b_φ of PVS/PVBTMA coacervates decrease, while those of PAA/PDMAEMA coacervates increase. In particular, the trend of τ_c over φ_e can be effectively captured by linear functions in semilog plots (Supplementary Fig. 9d and Supplementary Fig. 9e), in line with previous studies [10]. The τ_c is physically determined by an energy barrier E of associated interactions between stickers on polymer chains and environmental temperature T, as $\tau_c \sim \exp(E/k_\mathrm{B}T)$, where k_B is the Boltzmann constant [21]. With this relationship, these results suggests that interaction strength within coacervates scale linearly with the volume fraction of ethanol. Differently, the interaction strength within PAA/PDMAEMA coacervates increase over φ_e, while that within PVS/PVBTMA coacervates decreases.

Moreover, it is found that $G'$and G'' of these two coacervates monotonically decrease with increasing temperature (Supplementary Fig. 8). In addition, the critical frequency at which G' equals G'' shift toward higher frequencies, suggesting faster relaxation and more liquid-like properties at the high temperature (Supplementary Fig. 8). By applying a time-temperature superposition, frequency sweeps at different temperatures can be rescaled onto a single master curve using $T = 20$ ℃ as the reference point (Supplementary Fig. 10a and Supplementary Fig. 10b), with $w_{scale} = w\tau_c$, $G'_{scale} = G'_{scale}b_T$, and $G''_{scale} = G''_{scale}b_T$. It is observed that τ_c and b_T continually decrease with increasing temperature (Supplementary Fig. 10c). The trend of τ_c over T can be well fitted by the relationship of τ_c~exp $(E/k_{\mathrm{B}}T)$ in a semilog coordinate (Supplementary Fig. 10c). These results suggest that temperature can induce a melting of coacervates, regardless of their different sidechain compositions.

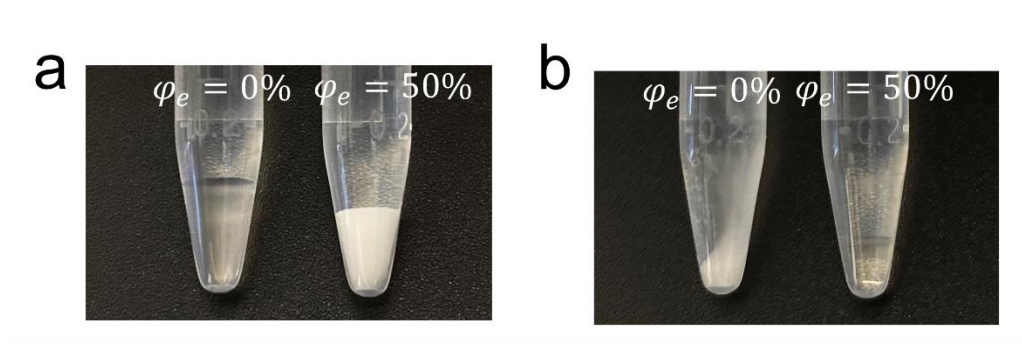

Supplementary Fig. 1. Photographs of (a) DEX-Sulf/DEAE-DEX (2.5 wt%/5 wt%) and (b) PSS/PDDA ($c_{\mathrm{m}} = 50$ mM and $c_{\mathrm{s}} = 1.5$ M) coacervates prepared at different volume fraction of ethanol ($\varphi_e = 0\%$ and $\varphi_e = 50\%$).

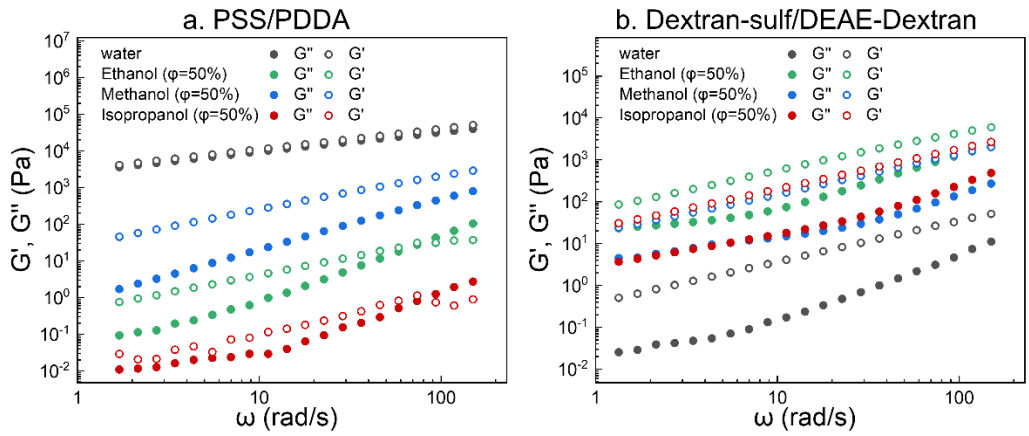

Supplementary Fig. 2. Frequency sweeps of (a) PSS/PDDA ($c_{\mathrm{m}} = 50$ mM and $c_{\mathrm{s}} = 1.5$ M) and (b) Dextran-sulf (2.5 wt%)/DEAE-Dextran (5 wt%), formed at four different solvent conditions: water, water/ethanol (1:1 v/v), water/methanol (1:1 v/v), and water/isopropanol (1:1 v/v).

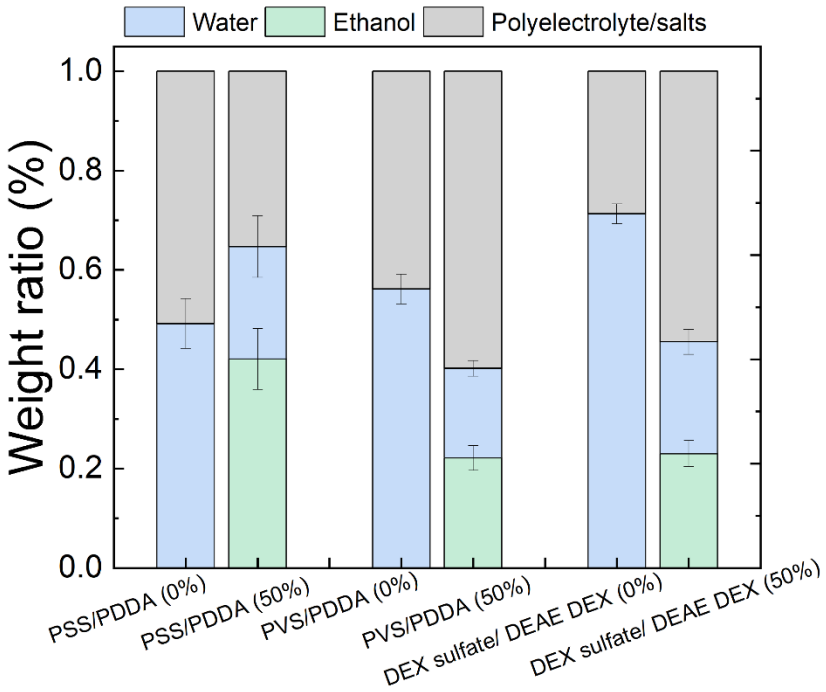

Supplementary Fig. 3. Thermogravimetric analysis of weight ratios of water, ethanol, and polyelectrolyte/salt in different types of coacervate phases at aqueous solution and water/ethanol (1:1 v/v) mixture. At least three independent samples are measured to calculate a mean value and standard deviation (error bars).

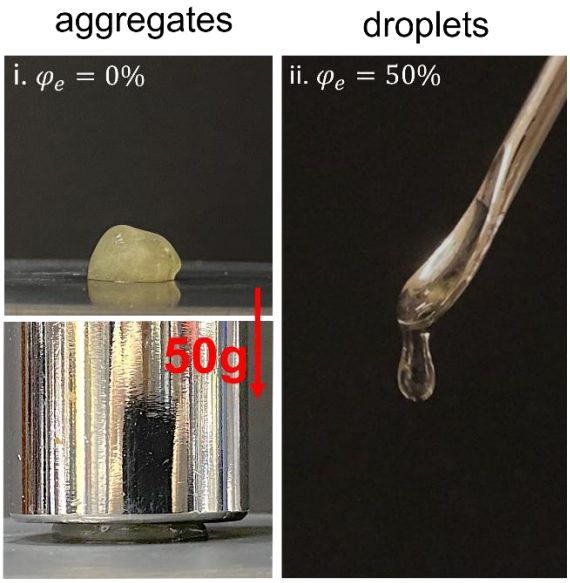

Supplementary Fig. 4. Photographs of PSS/PDDA coacervates formed at different volume fractions of ethanol. Coacervates exhibit as solid-like aggregates in pure water ($\varphi_e = 0\%$) and can bear heavy loads, while coacervates formed at $\varphi_e = 50\%$ v behave as liquid which readily drip off from a spoon.

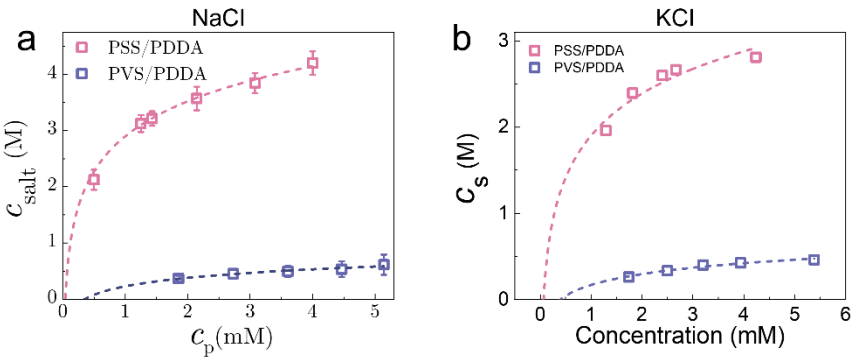

Supplementary Fig. 5. Left arms of phase diagram for PSS/PDDA (pink dash line) and PVS/PDDA (violet dash line) coacervates using (a) NaCI and (b) KCI salt.

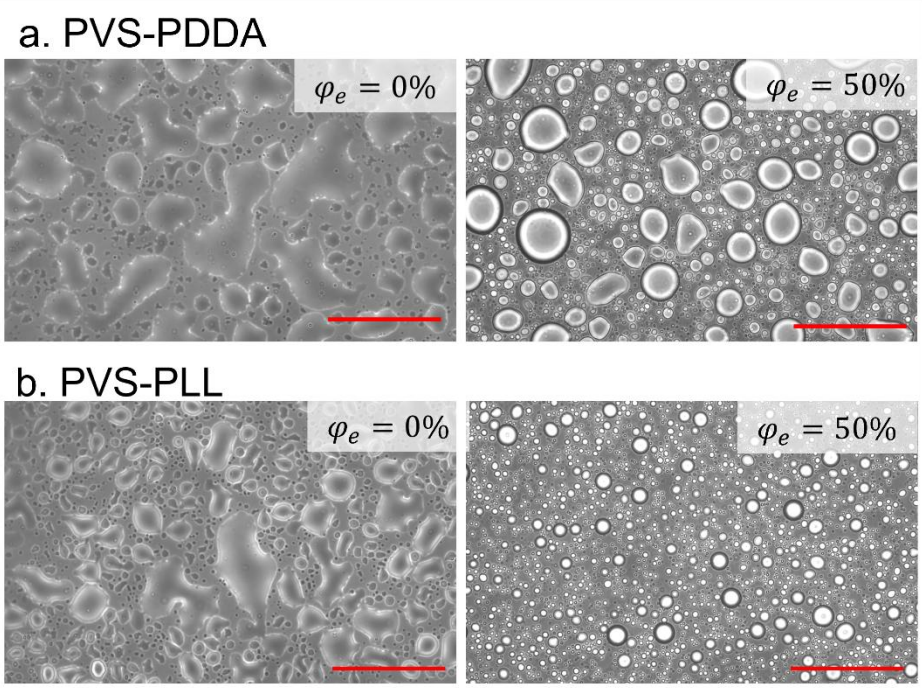

Supplementary Fig. 6. Bright-field images of (a) PVS/PDDA and (b) PVS/PLL coacervates. Images were acquired after depositing solutions onto cover slides and allowing approximately 10 minutes for complete wetting of coacervate droplets to the substrate. Scale bars: 100 μm.

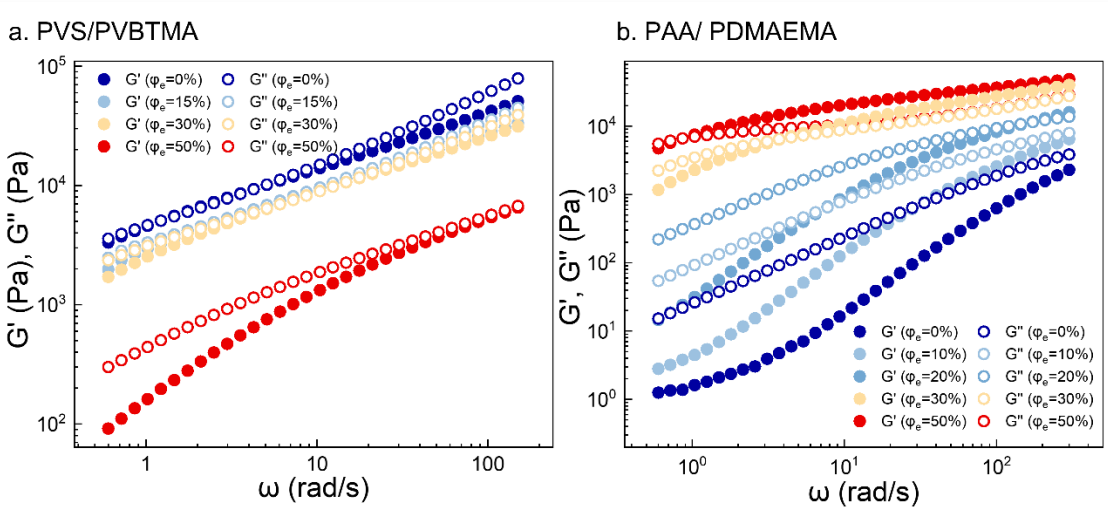

Supplementary Fig. 7. Frequency sweeps of (a) PVS/PVBTMA and (b) PAA/PDMAEMA coacervates at different volume fractions of ethanol (φ_e). The storage modulus G' and loss modulus G'' of PVS/PVBTMA coacervates monotonically decrease over φ_e, while that of PAA/PDMAEMA coacervate increase as φ_e increases.

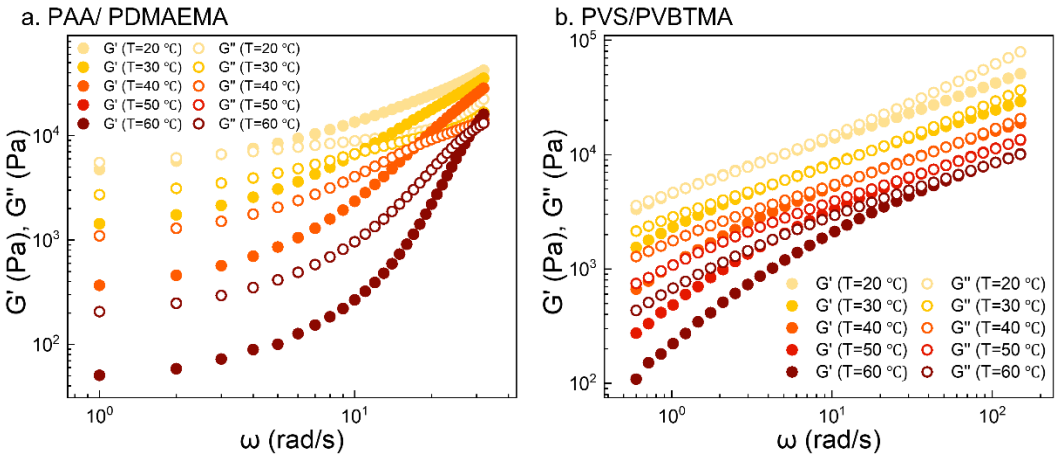

Supplementary Fig. 8. Frequency sweeps of (a) PAA/PDMAEMA and (b) PVS/PVBTMA at various temperatures. The storage modulus G' and loss modulus G'' of PAA/PDMAEMA and PVS/PVBTMA coacervates monotonically decrease with the increasing temperature.

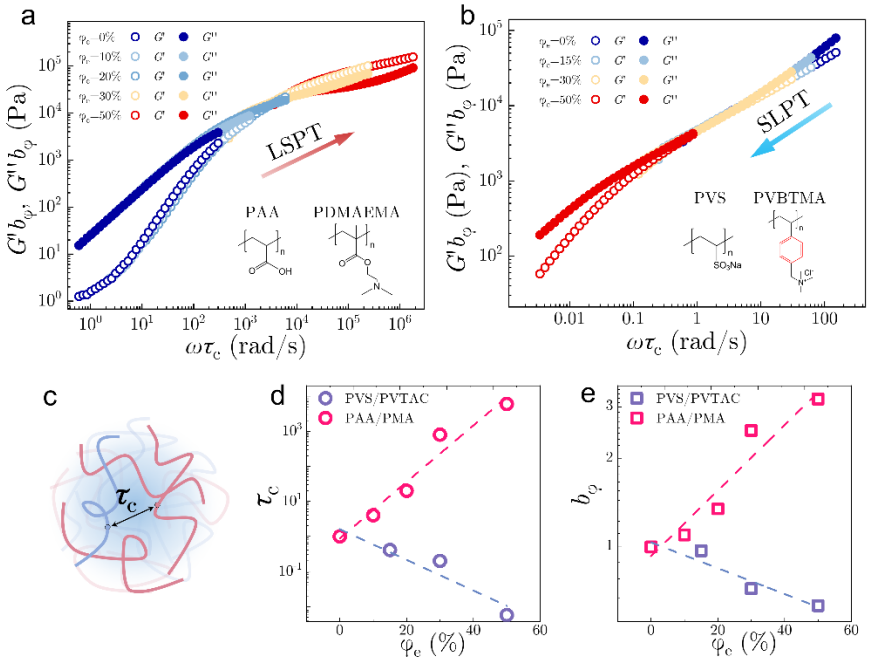

Supplementary Fig. 9. Time-alcohol superposition plots of (a) PAA/PDMAEMA and (b) PVS/PVBTMA complex coacervates. The insert images show the chemical structures of polyelectrolytes. The concentration of charged monomer c_m is 50 mM for all polyelectrolytes and coacervates are therefore formed at a neutral stoichiometry. Frequency sweeps conducted at various volume fractions of ethanol (φ_e) are used for the time-alcohol superposition (Supplementary Fig. 7). The LSPT and SLPT are identified for these two coacervates, respectively. (c) Schematic illustration of the critical relaxation time τ_c which is related to the interactions between associative residues. (d) (e) Values of the critical relaxation time τ_c and vertical shift factors b_φ as a function of φ_e. The dashed lines are linear fittings to experimental points in the semi-logarithmic plots.

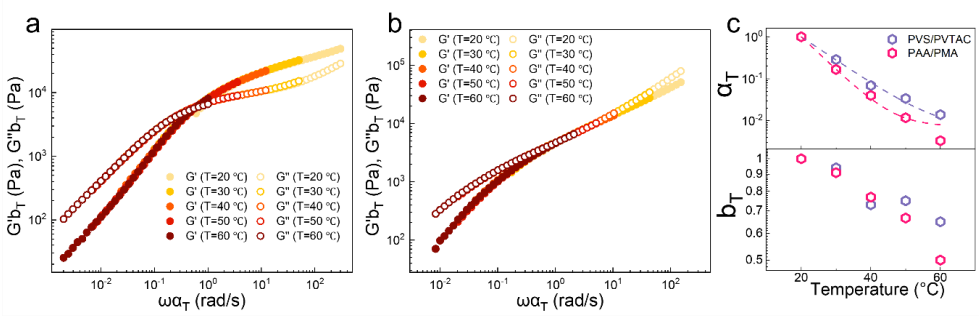

Supplementary Fig. 10. Rescaled frequency sweeps of (a) PAA/PDMAEMA and (b) PVS/PVBTMA at different temperatures by multiplying the frequency and modulus by horizontal and vertical shift factors, α_T and b_T, respectively. (c) Values of α_T and b_T as a function of temperature. Experimental data of α_T over T are fitted using the expression $\alpha = k\exp(E/k_BT)$ as indicated by the dash lines.

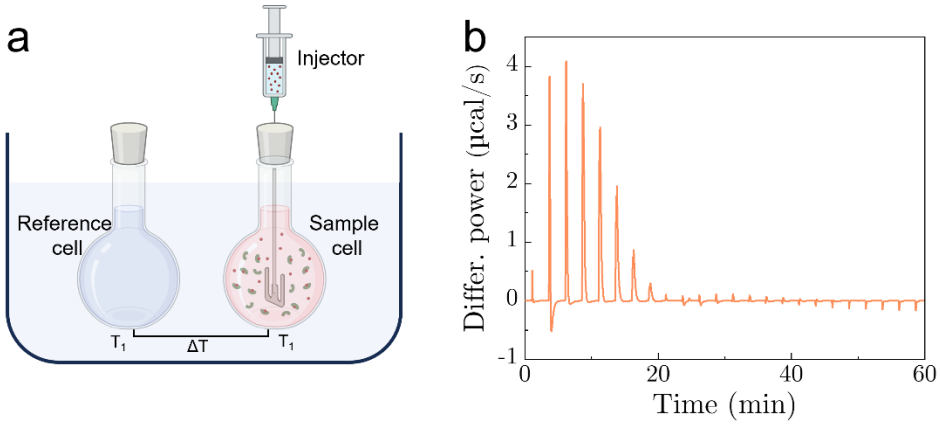

Supplementary Fig. 11. (a) Schematic illustration of configurations of isothermal titration calorimetry. (b) The differential power (DP) required to maintain a constant temperature for the isothermal injection of PVS ($c_m = 1$ mM) into a cell containing PLL ($c_m = 20$ mM).

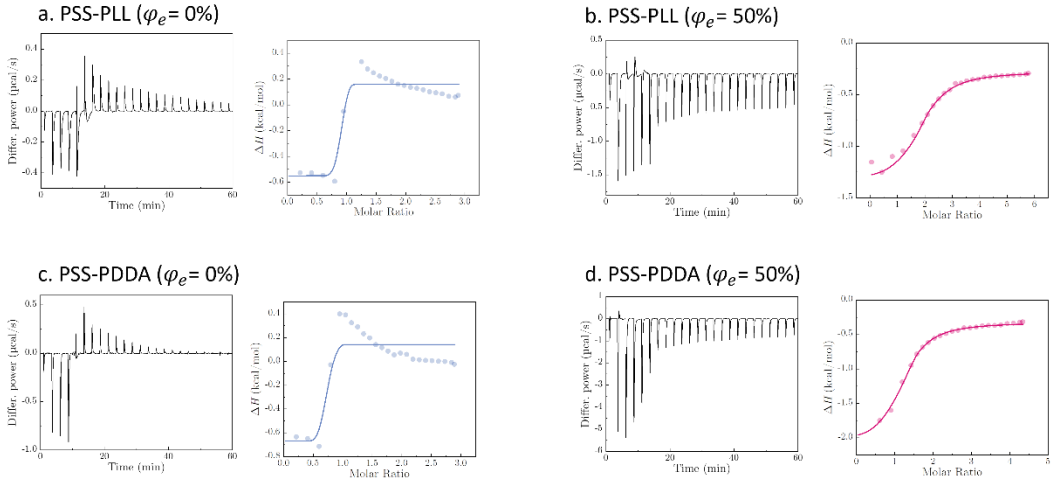

Supplementary Fig. 12. Plots of differential power (DP) signal versus time and enthalpy change ΔH versus time PSS/PLL and PSS/PDDA coacervate at $\varphi_e = 0\%$ and $\varphi_e = 50\%$. The experimental conditions are (a) PSS (0.5 mM), PLL (7.5 mM), and $\varphi_e = 0\%$; (b) PSS (0.5 mM), PLL (15 mM), and $\varphi_e = 50\%$; (c) PSS (0.5 mM), PDDA (7.5 mM), and $\varphi_e = 0\%$; (d) PSS (0.5 mM), PDDA (11.25 mM), and $\varphi_e = 50\%$.

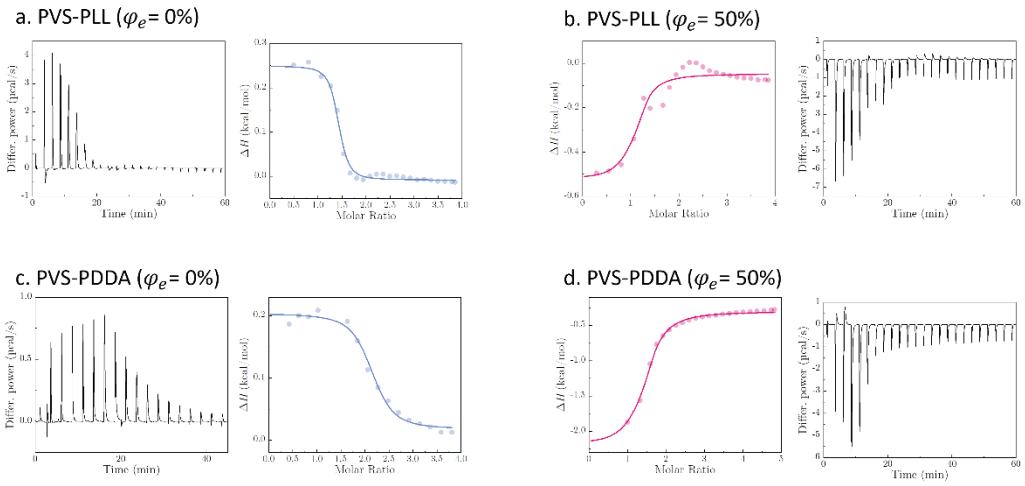

Supplementary Fig. 13. Plots of differential power (DP) signal versus time and enthalpy change ΔH versus time PSS/PLL and PSS/PDDA coacervate at $\varphi_e = 0\%$ and $\varphi_e = 50\%$. The experimental conditions are (a) PVS (1 mM), PLL (20 mM), and $\varphi_e = 0\%$; (b) PVS (1 mM), PLL (20 mM), and $\varphi_e = 50\%$; (c) PVS (1 mM), PDDA (20 mM), and $\varphi_e = 0\%$; (d) PVS (1 mM), PDDA (25 mM), and $\varphi_e = 50\%$.

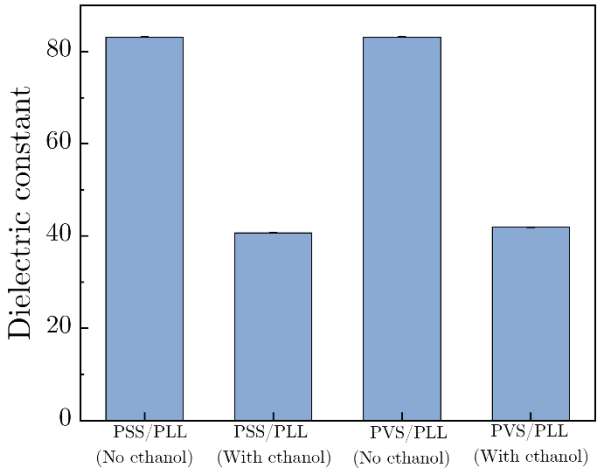

Supplementary Fig. 14. The computed values of dielectric constant of solutions containing oppositely charged monomers.

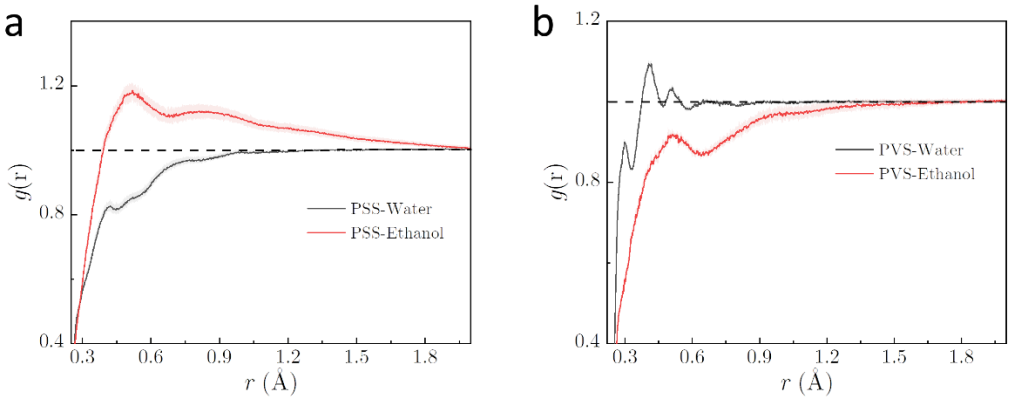

Supplementary Fig. 15. Radial distribution function of water (the dark lines) and ethanol (the red lines) molecules surrounding (a) PSS and (b) PVS, respectively.

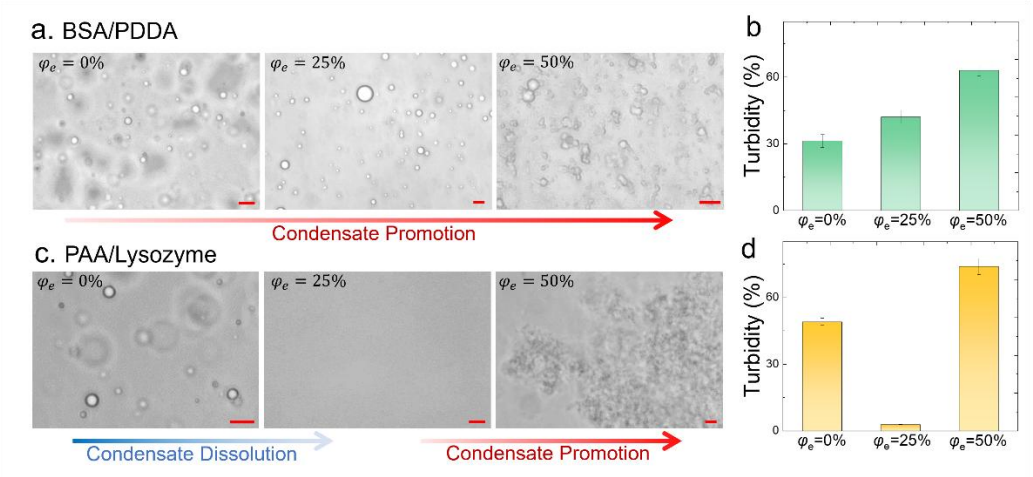

Supplementary Fig. 16. (a) Bright-field images and (b) solution turbidity showing that condensates formed by BSA (2 wt%) and PDDA (1 wt%) are promoted as φ_e increases. (c) Bright-field images and (d) solution turbidity showing that condensates formed by PAA (0.125 wt%) and Lysozyme (2 wt%) are firstly dissolved and then promoted to form solid-like aggregates with increasing φ_e. Scale bars are 20 μm.

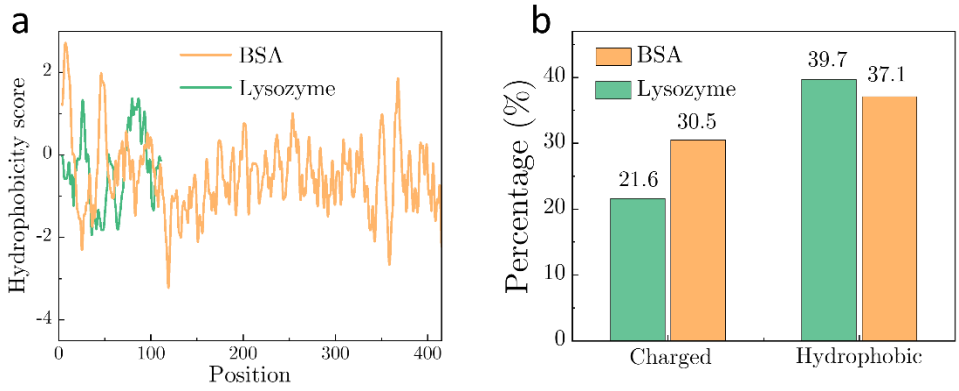

Supplementary Fig. 17. (a) Hydrophobicity scores and amino acid compositions of BSA and Lysozyme protein sequences using the Kyte-Doolittle scale [23].

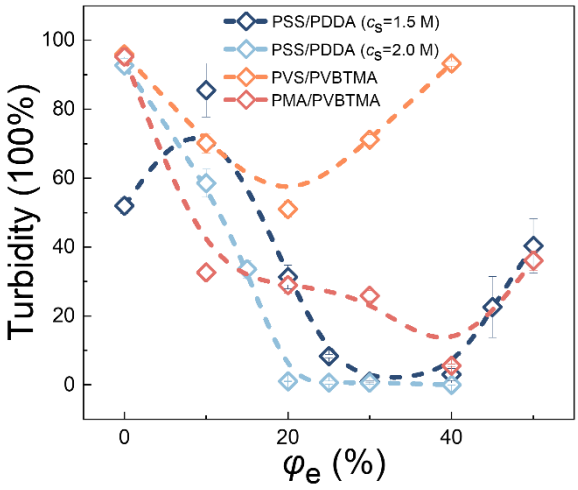

Supplementary Fig. 18. Solution turbidity of coacervates as a function of volume fraction of ethanol φ_e. These curves present a re-entrant phase separation of coacervates mediated by ethanol. Coacervates are PSS (50 mM)/PDDA (50 mM) with 1.5 M NaCI, PSS (50 mM)/PDDA (50 mM) with 2.0 M NaCI, PVS(50 mM)/PVBTMA(50 mM), and PMA(50 mM)/PVBTMA(50 mM), respectively.

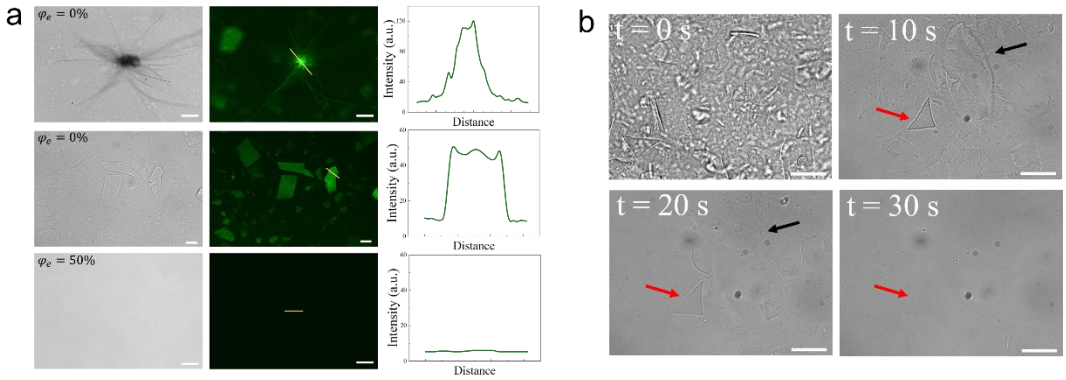

Supplementary Fig. 19. (a) Bright-field and fluorescence images of Aβ 1-42 plaques formed at different volume fraction of ethanol φ_e. Aβ 1-42 plaques were dyed by Thioflavin T (ThT). (b) Bright-field images showing the fast dissolution of Aβ 1-42 plaques by the introduction of ethanol at $\varphi_e = 50\%$. Scale bars are 20 μm.

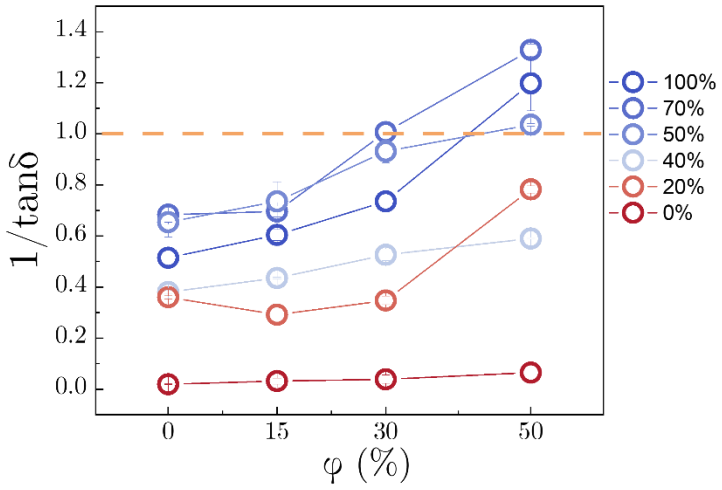

Supplementary Fig. 20. Plot of the inverse of loss factor 1/tanδ=G'/G'' as a function of ethanol volume fraction for coacervates prepared at different R values.

Reference

1. Matsui, A., et al., The Effect of Ethanol on Disassembly of Amyloid-β1-42 Pentamer Revealed by Atomic Force Microscopy and Gel Electrophoresis. International journal of molecular sciences, 2022. **23**(2): p. 889.

2. Ormeno, D., et al., Ethanol reduces amyloid aggregation in vitro and prevents toxicity in cell lines. Archives of medical research, 2013. **44**(1): p. 1-7.

3. Hansen, J., et al., Interactions in protein solutions close to liquid–liquid phase separation: ethanol reduces attractions via changes of the dielectric solution properties. Physical Chemistry Chemical Physics, 2021. **23**(39): p. 22384-22394.

4. Nemzer, L.R., et al., *Ethanol shock and lysozyme aggregation.* Soft Matter, 2013. **9**(7): p. 2187-2196.

5. Meng, S., et al., *Effect of mixed solvents on polyelectrolyte complexes with salt.* Colloid and Polymer Science, 2020. **298**(7): p. 887-894.

6. Zhao, Q., et al., Underwater contact adhesion and microarchitecture in polyelectrolyte complexes actuated by solvent exchange. Nature materials, 2016. **15**(4): p. 407-412.

7. Danielsen, S.P., et al., Complexation of a Conjugated Polyelectrolyte and Impact on Optoelectronic Properties. ACS Macro Letters, 2019. **8**(1): p. 88-94.

8. Murray, K.A., et al., Identifying amyloid-related diseases by mapping mutations in low-complexity protein domains to pathologies. Nature Structural & Molecular Biology, 2022: p. 1-8.

9. Jahan, I. and S.M. Nayeem, Effect of urea, arginine, and ethanol concentration on aggregation of 179CVNITV184 fragment of sheep prion protein. ACS omega, 2018. **3**(9): p. 11727-11741.

10. Sun, J., J.D. Schiffman, and S.L. Perry, *Linear Viscoelasticity and Time–Alcohol Superposition of Chitosan/Hyaluronic Acid Complex Coacervates.* ACS Applied Polymer Materials, 2022. **4**(3): p. 1617-1625.

11. Fu, J., H.M. Fares, and J.B. Schlenoff, *Ion-pairing strength in polyelectrolyte complexes.* Macromolecules, 2017. **50**(3): p. 1066-1074.

12. Gu, Y., et al., Contraction of weak polyelectrolyte multilayers in response to organic solvents. Soft Matter, 2016. **12**(6): p. 1859-1867.

13. McQuarrie, D.A., *Statistical mechanics*. 2000: Sterling Publishing Company.

14. Zhang, P. and Z.-G. Wang, *Interfacial structure and tension of polyelectrolyte complex coacervates.* Macromolecules, 2021. **54**(23): p. 10994-11007.

15. Debye, P., The theory of electrolytes. I. Lowering of freezing point and related phenomena. Physikalische Zeitschrift, 1923. **24**: p. 185-206.

16. Overbeek, J.T.G. and M. Voorn, *Phase separation in polyelectrolyte solutions. Theory of complex coacervation.* Journal of Cellular and Comparative Physiology, 1957. **49**(S1): p. 7-26.

17. Baruch Leshem, A., et al., *Biomolecular condensates formed by designer minimalistic peptides.* Nature Communications, 2023. **14**(1): p. 421.

18. Brangwynne, C.P., P. Tompa, and R.V. Pappu, *Polymer physics of intracellular phase transitions.* Nature Physics, 2015. **11**(11): p. 899-904.

19. Israelachvili, J.N., *Intermolecular and surface forces*. 2011: Academic press.

20. Jouyban, A., S. Soltanpour, and H.-K. Chan, *A simple relationship between dielectric constant of mixed solvents with solvent composition and temperature.* International journal of pharmaceutics, 2004. **269**(2): p. 353-360.

21. Spruijt, E., et al., Relaxation dynamics at different time scales in electrostatic complexes: time-salt superposition. Physical review letters, 2010. **105**(20): p. 208301.

22. Han, C.D. and J.K. Kim, On the use of time-temperature superposition in multicomponent/multiphase polymer systems. Polymer, 1993. **34**(12): p. 2533-2539.

23. Kyte, J. and R.F. Doolittle, *A simple method for displaying the hydropathic character of a protein.* Journal of molecular biology, 1982. **157**(1): p. 105-132.